

Goutam Ghoshal · Joseph A. Turner

Diffuse ultrasonic backscatter in a two-dimensional domain

Received: 4 November 2008 / Revised: 2 February 2009 / Published online: 21 April 2009
© Springer-Verlag 2009

Abstract The scattering of elastic waves in polycrystalline materials is relevant for ultrasonic materials characterization and nondestructive evaluation (NDE). Diffuse ultrasonic backscatter measurements are used widely to extract the microstructural parameters such as grain size and also to detect flaws in materials. Accurate interpretation of experimental data requires robust scattering models. Line transducers are often used for ultrasonic experiments such that an appropriate model for these two-dimensional problems is needed. Here, a theoretical expression for the temporal diffuse backscatter is derived for such domains under a single-scattering assumption. The result is given in terms of transducer and microstructural parameters. In addition, the problem is examined in terms of numerical simulations using Voronoi polycrystals that are discretized using finite elements in a plane-strain formulation. The material properties of the individual Voronoi cells are chosen according to appropriate material distributions. Such numerical models also allow scattering theories, including the one discussed here, to be examined for well-controlled microstructures. Example numerical results for materials with varying degrees of scattering that are of common interest are presented. The numerical results are compared with the theory developed with good agreement. These results are anticipated to impact ultrasonic NDE of polycrystalline media.

1 Introduction

Ultrasonic techniques are widely used to probe heterogeneous media. Often, these techniques rely on the scattering behavior of the waves that interact with the heterogeneous microstructure. Measurements of acoustic wave speeds, attenuations, and allowed acoustic polarizations can provide a means for material characterization [1–8]. Diffuse backscatter is one such method where the scattering of the ultrasonic wave is quantified to characterize the microstructure.

Diffuse ultrasonic backscatter involves quantifying the energy scattered at the grain boundaries that results from the mismatch of crystallite anisotropy. In a pulse/echo configuration the energy received between the frontwall and backwall echoes is termed the backscattered signal. This scattered signal is quantified by taking the variance of all the signals at various transducer positions keeping the distance between the transducer face and the front surface of the sample constant for all transducer positions, similar to an ultrasonic C-Scan experimental setup. Usually backscatter measurements are obtained in an immersion setup, using a focussed immersion transducer.

The transducer beam model is one of the major components needed in any theoretical description of such experiments. Cook [9] has given the solution to the linear wave equation for planar and plane-piston transducers in a polar coordinate system. Gubernatis et al. [10] presented the theory of ultrasound to detect flaws

G. Ghoshal · J. A. Turner (✉)
Department of Engineering Mechanics, W317.4 Nebraska Hall,
University of Nebraska-Lincoln, Lincoln, NE 68588-0526, USA
E-mail: jaturner@unl.edu

in an isotropic homogeneous elastic medium in a three-dimensional domain. The expression for the scattering amplitude is derived using the Green's function for an infinite medium. Thompson [11] calculated the pressure at the transducer face assuming a single medium for liquid–solid interfaces.

Margetan et al. [12] have given the backscatter model in three-dimensional domains supported by experimental results conducted on titanium alloys. The model is constructed assuming single scattering in the material. The model works well for low scattering material but may break down for high scattering materials or at very high frequencies where a higher order of scattering needs to be incorporated in the model. The scattered response depends very much on the input frequency of the wave and the scattering properties of the material. Thompson et al. [13] discussed the need for a theoretical model that includes multiple scattering for interpretation of experimental results. They also showed different configurations of the experimental setup to extract shear scattering properties of materials. Recently, Ghoshal et al. [14] derived the scattered response in a multiple scattering formalism and presented the solution for a single scattering assumption. Often multiple scattering problems cannot be solved analytically due to the complexity of the theory. It may be useful to simulate such experiments using numerical methods such as the finite element method, the finite difference or others to understand the scattering processes in materials. Here a finite element technique is used to simulate ultrasonic wave propagation in polycrystalline materials.

In various applications line transducers (transducer with a cylindrical focus) are often used for inspection of heterogeneous materials. These types of experiments can often be approximated as two-dimensional, especially for cases such as materials with elongated grains. Thus, an appropriate theoretical model is needed. Here, a two-dimensional model for backscatter measurement is derived within a single scattering formalism. The approach used follows that of Thompson et al. [11] for the singly scattered response (SSR) for polycrystalline materials in a three-dimensional domain.

The diffuse backscatter coefficient, which is proportional to the correlation length and the elastic properties of the material, is derived using the Green's function of the material. The transducer beam pattern is modeled using a single order Gaussian beam. The two-dimensional theoretical model for the scattered response is then compared with numerical results obtained from finite element technique. The numerical model for the polycrystalline material is constructed using a Voronoi tessellation of randomly distributed points. ABAQUS [15] is used to obtain the FEM solutions of wave propagation in Voronoi polycrystals. A plane-strain formulation is used with infinite boundary conditions at the sides. These infinite boundaries absorb the energy such that reflection is minimized [16,17].

2 Theory

The interest here is for studying ultrasonic wave propagation through a liquid–solid interface. But following Thompson [11], discussion begins with a fluid problem and later the reciprocity theorem is used to derive the diffuse ultrasonic scattered response in the solid for a wave propagating through a planar liquid–solid interface. The geometry considered here for the scattering calculation is shown in Fig. 1, where the distance r is from a point on the transducer line to the center of the scatterer and $2a$ is the length of the line transducer. Therefore, the origin of r varies across the transducer line. The velocity potential ϕ in a two-dimensional domain is given by

$$\phi = -\frac{i}{4} V_0 \int H_0(k_0 r) dr, \quad (1)$$

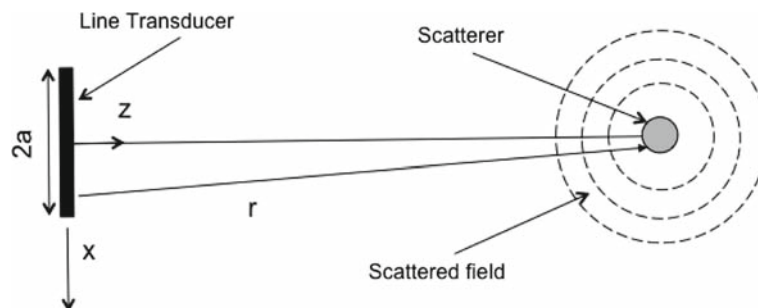


Fig. 1 Geometry of the scattering problem. Here the background is assumed to be a fluid

where V_0 is the initial velocity, k_0 the wave number and $H_0(r)$ is the Hankel function. The limit of the integration is along the transducer line. The harmonic time dependent term $e^{i\omega t}$ is suppressed in Eq. (1). Using the asymptotic representation of the Hankel function $H_0(k_0 r)$, the time derivative of the velocity potential is given by

$$\dot{\phi} = \exp(-i\pi/4) \frac{\omega V_0}{2\sqrt{2\pi k_0}} \int \frac{\exp(-ik_0 r)}{\sqrt{r}} dr. \quad (2)$$

Considering the flaw being on the axis of the propagating beam z and also far from the transducer face the wave front can be assumed to be a plane wave. Thus in the ‘‘quasiplane-wave’’ assumption, the incident velocity field in terms of a plane wave amplitude is given by

$$\dot{u}_I \simeq V_0 \Pi(z) \exp(-ik_0 z), \quad (3)$$

where $\Pi(z)$ is equal to the pressure at depth z , divided by the pressure $\rho_0 v_0 V_0 \exp(-ik_0 z)$, that would have been radiated if the transducer had infinite extent. Thus

$$\begin{aligned} \Pi(z) &= \frac{-\rho_0 \dot{\phi}}{\rho_0 v_0 V_0 \exp(-ik_0 z)} \\ &= \frac{k_0 \exp(ik_0 z - i\pi/4)}{2\sqrt{2\pi k_0}} \int \frac{\exp(-ik_0 r)}{\sqrt{r}} dr, \end{aligned} \quad (4)$$

where ρ_0 and v_0 are the density and sound speed, respectively, for the fluid. Then the farfield scattering is given by

$$\dot{u}_s = [A \dot{u}_I] \frac{\exp(-ikr)}{\sqrt{r}}, \quad (5)$$

where A is the scattering amplitude. The received voltage F is written by combining Eq. (5) with a quasiplane-wave approximation $p \simeq \rho_0 v_0 \dot{u}$ as

$$F \simeq \left(\gamma \frac{\rho_0 v_0 \dot{u}_I}{2a} \right) \int \frac{A \exp(-ik_0 r)}{\sqrt{r}} dr, \quad (6)$$

where γ is a constant of proportionality relating the average unperturbed pressure and voltage received and a is the transducer length. The integration range of Eq. (6) covers the length of the transducer. Combining Eqs. (3), (4) and (6) the received voltage is reduced to

$$F = (\gamma \rho_0 v_0 V_0) \Pi^2(z) \exp(-2ik_0 z) \left(\exp(-i\pi/4) \frac{A}{k_0 a} \sqrt{2\pi k_0} \right). \quad (7)$$

Using the analytical solution for the received voltage given in Eq. (7) for a fluid medium, the reciprocity theorem can be used to derive the scattered field in a solid medium. Therefore, using the reciprocity theorem and the derivation given by Thompson et al. [11] the change in the scattered signal due to a flaw or inhomogeneity is given by

$$\Gamma = \beta [T_{01a} \Pi_a P_a] [T_{01b} \Pi_b P_b] \left[\frac{\sqrt{2\pi} A \rho_1 v_1}{\sqrt{k_0 a \rho_0 v_0}} \right], \quad (8)$$

where the subscripts a and b refer to the transmitting and receiving transducer and $T_{01} = \frac{2\rho_0 v_0}{\rho_0 v_0 + \rho_1 v_1}$ is the interface transmission coefficient. Γ is related to the voltage and P is the propagation phase term. The change in the scattered signal may be written as

$$\begin{aligned} \Gamma(\omega) &= \beta T_{01}^2 \Pi^2(\omega, x_1, z_1) \exp[-2i(k_0 z_{0S} + k_1 z_1)] \\ &\quad \times \exp[-2(\alpha_0 z_{0S} + \alpha_1 z_1)] \left[\frac{\sqrt{2\pi} A \rho_1 v_1}{\sqrt{k_0 a \rho_0 v_0}} \right]. \end{aligned} \quad (9)$$

The reference geometry is defined by the reflected signal from a planar surface. Thus the reflected signal from a reference geometry is

$$\Gamma_{\text{ref}}(\omega) = \beta R_{00} D \exp[-2ik_0 z_{0R} - 2\alpha_0 z_{0R}], \quad (10)$$

where D is the diffraction coefficient, $R_{00} = \frac{\rho_0 v_0 - \rho_1 v_1}{\rho_0 v_0 + \rho_1 v_1}$ the reflection coefficient and z_{0R} is the distance between the planar surface and the transducer face. The field must be corrected using the diffraction constant as shown by various authors [18, 19]. Rogers [18] has given the Lommel diffraction correction integral expression using Fresnel diffraction approximations given by

$$D = \frac{k}{8a} \exp[ikz] \int_{-a}^a \int_{-a}^a H_0 \left(k \left(\sqrt{z^2 + (x - x_0)^2} \right) \right) dx dx_0. \quad (11)$$

In a pulse/echo system configuration a single transducer is used as both source and receiver such that

$$\begin{aligned} \Gamma_s(\omega, x_1, z_1) &= \frac{\sqrt{\pi} \beta A(\omega, x_1, z_1) \rho_1 v_1 T_{01}^2}{\sqrt{2k_0 a \rho_0 v_0}} \Pi^2(\omega, x_1, z_1) \\ &\times \exp[-2i(k_0 z_{0S} + k_1 z_1)] \\ &\times \exp[-2\alpha_0 z_{0S} - 2\alpha_1 z_1]. \end{aligned} \quad (12)$$

Next we define the Fourier transform pair of the reference signal by

$$\begin{aligned} R(t) &= \int_{-\infty}^{\infty} \Gamma_{\text{ref}}(\omega) \exp(i\omega t) d\omega, \\ \Gamma_{\text{ref}}(\omega) &= \frac{1}{2\pi} \int_{-\infty}^{\infty} R(t) \exp(-i\omega t) dt, \end{aligned} \quad (13)$$

and for the scattered signal by

$$\begin{aligned} S(t, x_1, z_1) &= \int_{-\infty}^{\infty} \Gamma_s(\omega, x_1, z_1) \exp(i\omega t) d\omega, \\ \Gamma_s(\omega, x_1, z_1) &= \frac{1}{2\pi} \int_{-\infty}^{\infty} S(t, x_1, z_1) \exp(-i\omega t) dt. \end{aligned} \quad (14)$$

The reference signal in complex form may be written as

$$\begin{aligned} R(t) &= E(t) \exp(i\omega_0 t), \\ \text{Re} [E(t) \exp(i\omega_0 t)] &= E(t) \cos(\omega t). \end{aligned} \quad (15)$$

Here, $E(t)$ is the envelope function necessary to match the front wall echo reflected from the front surface of the sample. To eliminate β from Eq. (12), Eq. (10) is solved for β and substituted. After substitution the scattered signal is

$$\begin{aligned} S(t, x_1, z_1) &= H(\omega_0, x_1, z_1) \int_{-\infty}^{\infty} d\omega \Gamma_{\text{ref}}(\omega) \\ &\times \exp[i(\omega t - 2k_0(z_{0S} - z_{0R}) - 2k_1 z_1)], \\ H(\omega_0, x_1, z_1) &= \frac{\sqrt{2\pi} T_{01}^2 A(\omega_0, x_1, z_1) \rho_1 v_1}{R_{00} D(\omega_0) \sqrt{k_1 a \rho_0 v_0}} \Pi^2(\omega_0, x_1, z_1) \\ &\times \exp[2\alpha_0(z_{0R} - z_{0S}) - 2\alpha_1 z_1]. \end{aligned} \quad (16)$$

The attenuation coefficients α_0 and α_1 are evaluated at $\omega = \omega_0$ for the fluid and solid medium, respectively. Using $k = \omega/v$, the exponential term in integrand in Eq. (16) is written as $\exp[j\omega(t - t_0)]$, and

$$t_0 = 2 \frac{z_{0S} - z_{0R}}{v_0} + \frac{2z_1}{v_1} \quad (17)$$

denotes the time delay between the reference and the scattered signal. The integral in Eq. (16) is evaluated using Eqs. (13) and (15). The equation for S is then

$$S(t, x_1, z_1) = H(\omega_0, x_1, y_1, z_1) E(t - t_0) \times \exp[i\omega_0(t - t_0)]. \quad (18)$$

The total voltage is the sum of the scattered signal over the number of grains as

$$V(t) = \sum_{i=1}^m S_i(t, x_{1i}, z_{1i}). \quad (19)$$

The normalized scattered response $\Phi(t)$ is the variance of the measured noise voltage normalized by the peak amplitude square of the reference signal E_{\max} given by

$$\Phi(t) = \frac{\langle [\text{Re}(V(t))]^2 \rangle - \langle \text{Re}(V(t)) \rangle^2}{E_{\max}^2} \approx \frac{\langle [\text{Re}(V(t))]^2 \rangle}{E_{\max}^2}, \quad (20)$$

since a good diffuse field measurement is designed so that the mean response $\langle \text{Re}(V(t)) \rangle$ vanishes. The real part of the voltage may be written as

$$\begin{aligned} \text{Re}(V(t)) &= \sum_{i=1}^m \text{Re}[S_i] = \sum_{i=1}^m |B_i| \cos(\omega_0 t + \phi_i), \\ |B_i| &= |H_i(\omega_0, x_{1i}, z_{1i}) E(t - t_{0i})|, \\ \phi_i &= -\omega_0 t_{0i} + \text{phase of } H_i. \end{aligned} \quad (21)$$

Therefore $\langle [\text{Re}(V(t))]^2 \rangle$ is non zero for $i = j$,

$$\langle [\text{Re}(V(t))]^2 \rangle = \frac{1}{2} \sum_{i=1}^m \langle |B_i|^2 \rangle. \quad (22)$$

The summation is the area of each grain multiplied by n grains,

$$\sum_{i=1}^m \approx n \iint dx_1 dz_1. \quad (23)$$

Then the SSR is written

$$\begin{aligned} \Phi(t) &= |\sqrt{n}A(\omega_0)|^2 \left(\frac{\sqrt{\pi} T_{01}^2 \rho_1 v_1 \exp(2\alpha_0(z_{0R} - z_{0S}))}{R_{00} D(\omega_0) \sqrt{k_1 a \rho_0 v_0}} \right)^2 \\ &\times \int \Psi(z_1) \left| \frac{E(t - t_0)}{E_{\max}} \right|^2 \exp[-4\alpha_1 z_1] dz_1, \end{aligned} \quad (24)$$

where $|\sqrt{n}A(\omega_0)|$ is termed the diffuse backscattered coefficient, $\Psi(z) = \int_{-\infty}^{\infty} |\Pi(\omega, x, z)|^4 dx$, is proportional to the transducer beam energy along a line at depth z and \sqrt{n} is the area density of grains.

The different components of the SSR $\Phi(t)$ are derived in detail in the following sections. The diffuse backscatter coefficient is related to the material properties and $\Psi(z)$ accounts for the transducer beam pattern in the material. The SSR is a dimensionless quantity normalized by the peak amplitude of the reference signal.

2.1 Diffuse backscatter coefficient

The diffuse backscatter coefficient is proportional to the material properties and the microstructure of the material. The microstructure can be described by the grain size distribution. The spatial correlation function is usually used to define a polycrystalline microstructure. For example a two point correlation function for a polycrystalline material gives the probability of any two points lying in the same grain. The diffuse backscatter coefficient is also a measure of the covariance of the elastic moduli tensor. Equation (24) can be used either to obtain microstructural information by knowing the material properties or to obtain the material properties by knowing the microstructure. The diffuse backscatter coefficient is a function of the scattered amplitude and grain area density.

The scattered displacements [10] in terms of the Green's function are given by

$$u_i^s = \delta\rho\omega^2 \int_{R_2} dA' g_{im} u_m + \delta C_{ijklm} \int_{R_2} dA' g_{ij,k} u_{l,m}, \quad (25)$$

where u_l is the displacement field in a flawless elastic medium, g_{im} is the Green's function of the medium and δC_{ijklm} denotes the fluctuations in the elastic constants. The scalar Green's function in a two-dimensional domain is given by [20]

$$\mathbf{g}(\mathbf{r}, \mathbf{r}') = \frac{j}{4} H_0^{(1)}(j\mathbf{k} \cdot |\mathbf{r} - \mathbf{r}'|). \quad (26)$$

For an elastic isotropic material, the Green's function for an infinite volume [21] is

$$\mathbf{g}(\mathbf{r} - \mathbf{r}') = -\frac{j}{4\rho\omega^2} [\beta^2 H_0(\beta R) - \nabla\nabla \cdot (H_0(\alpha R) - H_0(\beta R))]. \quad (27)$$

Using the asymptotic representation of the Hankel function, the longitudinal component of the Green's function is

$$g_{ij}(\mathbf{r} - \mathbf{r}') = -\frac{1}{4\rho\omega^2} \sqrt{\frac{2}{\pi}} \left[\frac{\beta^2 \exp(i\beta R)}{\sqrt{\beta} \sqrt{R}} \delta_{ij} - \frac{\partial}{\partial x_i} \frac{\partial}{\partial x_j} \left(\frac{\exp(i\alpha R)}{\sqrt{\alpha R}} - \frac{\exp(i\beta R)}{\sqrt{\beta R}} \right) \right], \quad (28)$$

where $R = |\mathbf{r} - \mathbf{r}'|$. As $kr \rightarrow \infty$, $(kR)^{-1/2} \sim (kr)^{-1/2}$ and $(kR) \sim \left(k \left(r - \frac{(\mathbf{r} \cdot \mathbf{r}')}{r}\right)\right)$. The derivatives can then be approximated as

$$\begin{aligned} \frac{\partial}{\partial x_i} \frac{\exp(ikR)}{\sqrt{R}} &\sim (-ik) \frac{\exp(ikr)}{\sqrt{r}} \hat{r}_i \exp(-i\mathbf{k} \cdot \mathbf{r}'), \\ \frac{\partial}{\partial x_i} \frac{\partial}{\partial x_j} \frac{\exp(ikR)}{\sqrt{R}} &\sim (-ik)^2 \frac{\exp(ikr)}{\sqrt{r}} \hat{r}_i \hat{r}_j \exp(-i\mathbf{k} \cdot \mathbf{r}') \sim -k^2 \frac{\exp(ikr)}{\sqrt{r}} \hat{r}_i \hat{r}_j \exp(-i\mathbf{k} \cdot \mathbf{r}'), \\ \frac{\partial}{\partial x_i} \frac{\partial}{\partial x_j} \frac{\partial}{\partial x_k} \frac{\exp(ikR)}{\sqrt{R}} &\sim (-ik)^3 \frac{\exp(ikr)}{\sqrt{r}} \hat{r}_i \hat{r}_j \hat{r}_k \exp(-i\mathbf{k} \cdot \mathbf{r}') \sim ik^3 \frac{\exp(ikr)}{\sqrt{r}} \hat{r}_i \hat{r}_j \hat{r}_k \exp(-i\mathbf{k} \cdot \mathbf{r}'). \end{aligned} \quad (29)$$

Substituting the above into the Green's function expression, Eq. (28), yields

$$\begin{aligned} g_{ij} &= -\frac{1}{4\rho\omega^2} \sqrt{\frac{2}{\pi}} \left[\frac{\beta^2 \exp(i\beta r)}{\sqrt{\beta} \sqrt{r}} \exp(-i\boldsymbol{\beta} \cdot \mathbf{r}') \{\delta_{ij} - \hat{r}_i \hat{r}_j\} \right. \\ &\quad \left. + \frac{1}{4\rho\omega^2} \sqrt{\frac{2}{\pi}} \left[\frac{\alpha^2 \exp(i\alpha r)}{\sqrt{\alpha} \sqrt{r}} \hat{r}_i \hat{r}_j \exp(-i\boldsymbol{\alpha} \cdot \mathbf{r}') \right] \right]. \end{aligned} \quad (30)$$

The spatial derivative of the Green's function is then given by

$$\begin{aligned} -g_{ij,k} &= \frac{1}{4\rho\omega^2} \sqrt{\frac{2}{\pi}} \left[\frac{\beta^2 \exp(i\beta r)}{\sqrt{\beta} \sqrt{r}} \exp(-i\boldsymbol{\beta} \cdot \mathbf{r}') \{\delta_{ij} - \hat{r}_i \hat{r}_j\} \right] (-i\beta) \hat{r}_k \\ &\quad + \frac{1}{4\rho\omega^2} \sqrt{\frac{2}{\pi}} \left[\frac{\alpha^2 \exp(i\alpha r)}{\sqrt{\alpha} \sqrt{r}} \hat{r}_i \hat{r}_j \exp(-i\boldsymbol{\alpha} \cdot \mathbf{r}') \right] (-i\alpha) \hat{r}_k. \end{aligned} \quad (31)$$

The displacements are then written as

$$\begin{aligned}
-u_i^s = & \frac{1}{4\rho\omega^2} \sqrt{\frac{2}{\pi}} \frac{\beta^2}{\sqrt{\beta}} \left[\delta\rho\omega^2 \int_{R_2} dA' \left[\frac{\exp(i\beta r)}{\sqrt{r}} \exp(-i\boldsymbol{\beta}\cdot\mathbf{r}') \{ \delta_{im} - \hat{r}_i \hat{r}_m \} + \right] u_m \right. \\
& \left. + (-i\beta) \delta C_{ijklm} \int_{R_2} dA' \left[\frac{\exp(i\beta r)}{\sqrt{r}} \exp(-i\boldsymbol{\beta}\cdot\mathbf{r}') \{ \delta_{ij} - \hat{r}_i \hat{r}_j \} \hat{r}_k \right] u_{l,m} \right] \\
& + \frac{1}{4\rho\omega^2} \sqrt{\frac{2}{\pi}} \frac{\alpha^2}{\sqrt{\alpha}} \left[\delta\rho\omega^2 \int_{R_2} dA' \left[\frac{\exp(i\alpha r)}{\sqrt{r}} \hat{r}_i \hat{r}_m \exp(-i\boldsymbol{\alpha}\cdot\mathbf{r}') \right] u_m \right. \\
& \left. + (-i\alpha) \delta C_{ijklm} \int_{R_2} dA' \left[\frac{\exp(i\alpha r)}{\sqrt{r}} \hat{r}_i \hat{r}_j \exp(-i\boldsymbol{\alpha}\cdot\mathbf{r}') \right] \hat{r}_k u_{l,m} \right]. \tag{32}
\end{aligned}$$

Defining $f_i(k)$ as

$$\begin{aligned}
f_i(k) = & -\frac{1}{4\rho\omega^2} \frac{k^2}{\sqrt{k}} \sqrt{\frac{2}{\pi}} \left[\delta\rho\omega^2 \int_{R_2} dA' u_i \exp(-i\mathbf{k}\cdot\mathbf{r}') \right. \\
& \left. + (-ik\hat{r}_j) \delta C_{ijklm} \int_{R_2} dA' u_{l,m} \exp(-i\boldsymbol{\alpha}\cdot\mathbf{r}') \right], \tag{33}
\end{aligned}$$

the scattered displacement field may then be written as

$$u_i^s \sim \hat{r}_i \hat{r}_j f_j(\alpha) \frac{\exp(i\alpha r)}{\sqrt{r}} + (\delta_{ij} - \hat{r}_i \hat{r}_j) f_j(\beta) \frac{\exp(i\beta r)}{\sqrt{r}}. \tag{34}$$

The incident wave field and its spatial derivative are

$$\begin{aligned}
u_i^0 &= \exp(ikr), \\
u_{i,j} &= ik u_i^0. \tag{35}
\end{aligned}$$

In the direction of the wave propagation, the longitudinal mode is

$$f_2(k) \frac{\exp(i\alpha r)}{\sqrt{r}} = -\frac{1}{4\rho\omega^2} \frac{k^2}{\sqrt{k}} \sqrt{\frac{2}{\pi}} \left[(\delta\rho\omega^2 + k^2 \hat{r}_3 \delta C_{3333}) \int_{R_2} dA' \exp(2ikr) \right] \frac{\exp(-i\mathbf{k}\cdot\mathbf{r}')}{\sqrt{r}}, \tag{36}$$

such that the scattered amplitude is

$$A = -\frac{1}{4\rho\omega^2} \frac{k^2}{\sqrt{k}} \sqrt{\frac{2}{\pi}} \left[(\delta\rho\omega^2 + k^2 \delta C_{3333}) \int_{R_2} dA' \exp(2i\mathbf{k}\cdot\mathbf{r}') \right]. \tag{37}$$

Assuming constant density in the material $\delta\rho = 0$, and the scattered amplitude reduces to

$$A = -\frac{1}{4\rho V^2} \frac{k^2}{\sqrt{k}} \sqrt{\frac{2}{\pi}} \left[\delta C_{3333} \int d^2x \exp(2ikz) \right]. \tag{38}$$

The backscatter coefficient $\eta(\omega)$ is proportional to the square of the scattered amplitude and is given by

$$\eta(\omega) = \frac{1}{k} \left(\frac{k^2}{2\sqrt{2\pi}\rho V^2} \right)^2 \langle \delta C_{3333}(\mathbf{r}) \delta C_{3333}(\mathbf{r}') \rangle \times \left[\int d^2s W(s) \exp(2iks) \mathbf{k} \right], \quad (39)$$

where $W(s) = \exp\left(-\frac{|s|}{L}\right)$ is the two-point spatial correlation function with the correlation length L (typically on the order of the grain diameter). Evaluating the integral gives the expression for the diffuse backscatter coefficient as

$$\eta(\omega) = \frac{1}{k} \left(\frac{\omega^2}{2\rho V^4} \right)^2 \langle \delta C_{3333}^2 \rangle \left[\frac{L^2}{(1 + 4k^2 L^2)^{3/2}} \right]. \quad (40)$$

Weaver [22] showed that the correlation length varies in the high frequency limit as the scattering increases with frequency. Of particular interest here is to fit the diffuse backscatter model shown in Eq. (24) with two-dimensional numerical results by varying the correlation length and to investigate its dependence as a function of frequency.

2.2 Gaussian beam model

The backscatter model as shown in Eq. (24) is proportional to the transducer beam characteristics. Schmerr [23] modeled the transducer beam pattern using both single and multiple Gaussian functions. The multi-Gaussian model is used to fit the side lobes of the transducer beam profile, whereas a single Gaussian profile fits the central lobe with acceptable accuracy. Other models such as a Gauss–Hermite [9,24] can also be used to derive the ultrasonic field strength from a focussed transducer. The single Gaussian beam model is used here for simplicity.

The square of the transducer beam energy from a line of grains at depth z is given by

$$\Psi(z) = \int_{-\infty}^{\infty} \int_{-\infty}^{\infty} |\Pi(\omega, x, z)|^4 dx, \quad (41)$$

where $\Pi(\omega, x, y, z)$ is the measure of the ultrasonic field strength. The displacement at the field point is given by

$$\mathbf{U} = \mathbf{d}U_0 T \exp[j(\omega t - k_0 z_0 - k_1 z_1)] \exp[-\alpha_0 z_0 - \alpha_1 z_1] \Pi, \quad (42)$$

where \mathbf{d} is the polarization vector, U_0 the initial displacement amplitude, T the transmission coefficient, $\exp[j(\omega t - k_0 z_0 - k_1 z_1)]$ the plane wave phase propagation, $\exp[-\alpha_0 z_0 - \alpha_1 z_1]$ the attenuation term, and the remaining factor is defined as Π . Here z_0 and z_1 are the propagation distances in the coupling medium and solid, respectively. Under a Gaussian beam approximation, the displacement field is

$$\mathbf{U}(x, z, t) = \mathbf{d}_z A \left[\frac{w(0)}{w(z)} \right]^{1/2} \exp[j(\omega t - kz) - \alpha z] \times \exp[j\{\psi(z) - \psi(0)\}] \exp\left[-j \left\{ \frac{kx^2}{2q(z)} \right\}\right], \quad (43)$$

where A is the amplitude of the Gaussian beam. Comparing Eq. (43) to (42) the expression for $\Pi(\omega, x, y, z)$ is

$$\Pi(\omega, x, z) = 1.77 \left[\frac{w(0)}{w(z)} \right]^{1/2} \exp[j\{\psi(z) - \psi(0)\}] \times \exp\left[-j \left\{ \frac{kx^2}{2q(z)} \right\}\right], \quad (44)$$

where $w(z)$ is the width of the Gaussian profile, $R(z)$ the radius of curvature of the wavefront, $\psi(z)$ the phase and $q(z)$ is a complex radius of curvature incorporating the beam width and the real value of the radius of curvature. The values for the initial width of the beam $w(0)$ and the value 1.77 in Eq. (44) are chosen by fitting the axial and the lateral beam pattern of a focussed ultrasonic transducer with a single Gaussian model [25]. The Gaussian beam complex parameters are defined as

$$\begin{aligned} q(z) &= q(0) + z, \\ \frac{1}{q(z)} &= \frac{1}{R(z)} - j \frac{\lambda}{\pi w^2(z)}, \\ R(0) &= -F \quad \text{and} \quad w(0) = 0.7517a, \\ R(z) &= \frac{1}{\text{Re}[1/q(z)]}, \end{aligned} \quad (45)$$

where F is the focal length of the transducer. The excess phase $\psi(z)$ and the Gaussian beam width $w(z)$ as a function of depth z are defined as

$$\begin{aligned} \psi(z) &= \left(\frac{1}{2}\right) \left[\frac{\pi}{2} - \tan^{-1} \left(\frac{\text{Im}(q(z))}{\text{Re}(q(z))} \right) \right], \\ w(z) &= \left[\frac{-\lambda/\pi}{\text{Im}(1/q(z))} \right]^{1/2}, \end{aligned} \quad (46)$$

where $\psi(z)$ and $w(z)$ are real values. The magnitude of Π then becomes

$$|\Pi(\omega, x, z)| = 1.77 \left[\frac{w(0)}{w(z)} \right]^{1/2} \exp \left[- \left(\frac{x}{w(z)} \right)^2 \right]. \quad (47)$$

Therefore

$$\Psi(z) = \int_{-\infty}^{\infty} |\Pi(\omega, x, z)|^4 dx = 4.9150 \left[\frac{a^2}{w(z)} \right]. \quad (48)$$

$\Psi(z)$ takes into account the variations of the field strength of the beam as a function of depth z in the test material, which is inversely proportional to the Gaussian beam width as a function of depth as shown in Eq. (48).

The final expression for the SSR can be written as

$$\begin{aligned} \Phi(t) &= \left(\frac{\sqrt{\pi} T_{01}^2 \rho_1 v_1 \exp(2\alpha_0(z_{0R} - z_{0S}))}{R_{00} D(\omega_0) \sqrt{k_1} a \rho_0 v_0} \right)^2 \\ &\times \left[\frac{1}{k} \left(\frac{\omega^2}{2\rho V^4} \right)^2 \langle \delta C_{33}^2 \rangle \left(\frac{L^2}{(1 + 4k^2 L^2)^{3/2}} \right) \right]^2 \\ &\times \int 4.9150 \left[\frac{a^2}{w(z)} \right] \left| \frac{E(t - t_0)}{E_{\max}} \right|^2 \exp[-4\alpha_1 z_1] dz_1. \end{aligned} \quad (49)$$

In the following section the numerical results are discussed in detail. Since in the numerical model the coupling medium is not present the above formulation for the scattered response is modified accordingly.

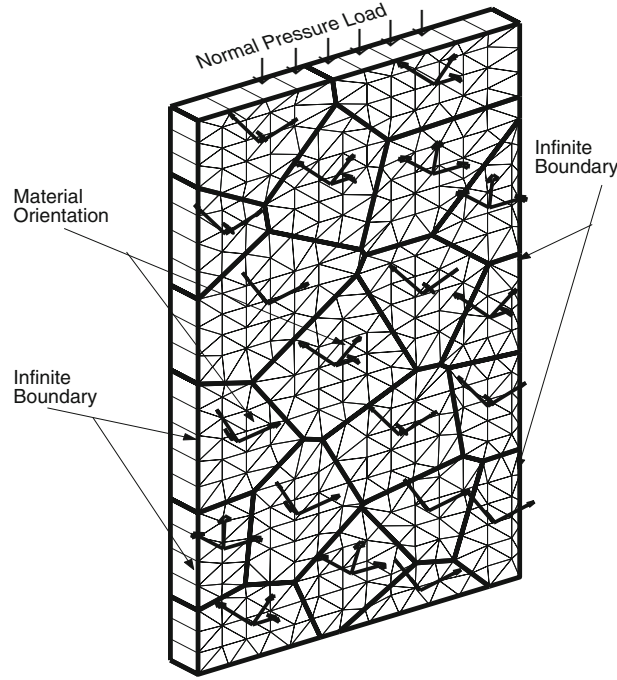


Fig. 2 Numerical model for polycrystalline material

3 Numerical results

The numerical polycrystalline models used here are constructed using a Voronoi tessellation from uniformly distributed points with the distance between the points being restricted to obtain a uniform grain size distribution. Here, Voronoi polycrystals are created inside the required finite domain using the “Method of Virtual Nuclei” [16, 17, 26], an algorithm to construct Voronoi polycrystals inside a finite domain with convex boundaries. The two-dimensional Voronoi polycrystals are constructed and discretized into finite triangular elements of $50\ \mu\text{m}$. The elements in each crystal are assigned a random material orientation in the three crystal directions. Thus, the model is not completely two-dimensional, rather it is a pseudo-three-dimensional model. Since the displacement in the out of plane axis is constrained the scattered response can still be approximated using a two-dimensional wave theory derived in the previous section. An example model is shown in Fig. 2. For clarity, Fig. 2 was created with large crystals and elements. Plane strain boundary conditions are chosen by restricting the displacement of all the nodes in the out-of-plane direction. The extrusion of the triangular elements facilitates to have three-dimensional crystal orientation. Due to the plane strain formulation there is no displacement in the out of plane axis even though the elements are in the three-dimensional domain. The prism elements are helpful for avoiding the difficulties of mapping the crystal orientation to the two-dimensional domain. Material orientation is indicated in Fig. 2 by the local coordinate axes shown for each crystal. The use of the infinite elements at the vertical boundaries of the model minimizes reflections of the wave from these boundaries. The boundary conditions at the top and bottom of the model are stress free. The displacement of the nodes at the loading area is stored for the backscatter calculation. The snapshot of the finite element simulation is shown in Fig. 3, at various time steps for a model size of 8 mm by 12 mm and depth of 0.75 mm in the out of axis direction.

The normalized scattered response is the variance of the signals given by [12]

$$\Phi(t) = \frac{\langle u^2 \rangle - \langle u \rangle^2}{E_{\max}^2}, \quad (50)$$

where u is the nodal displacement and $\langle y \rangle$ denotes the mean of y . The scattered response is normalized by the peak amplitude of the front surface echo E_{\max} . A typical signal at a nodal point in aluminum at the loading area is shown in Fig. 4. The frontwall and backwall echoes are evident. The main region of interest for the backscatter calculation is the signal between the front and the back wall echoes.

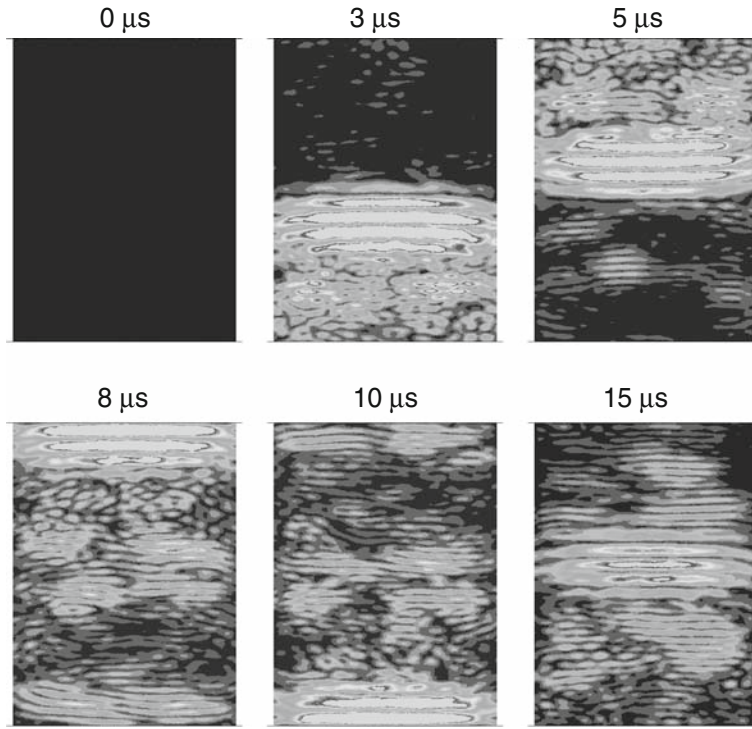


Fig. 3 Simulation for aluminum with heterogeneous material properties (600 crystals in a 5 mm by 12 mm model for 5 MHz of longitudinal input wave)

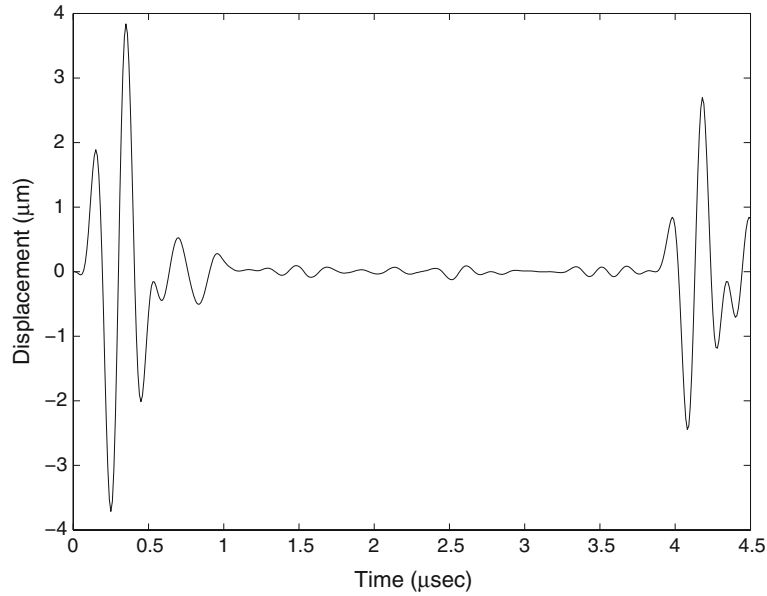


Fig. 4 Single nodal displacement for three cycle 5 MHz input wave

The pressure load applied in the numerical model is similar to a contact transducer. From Eq. (24), the scattered response signal in a single medium without any interface is

$$\Phi(t) = \eta(\omega_0)^2 \frac{\pi}{ka^2} \times \int \Psi(z) \left| \frac{E(t-t_0)}{E_{\max}} \right|^2 \exp[-4\alpha z] dz. \quad (51)$$

The integral is converted into a time domain integral using $z = \frac{v_1}{2} (t - \tau)$ as

$$\Phi(t) = \eta(\omega_0)^2 \frac{\pi}{ka^2} \times \frac{v_1}{2} \int_{\tau_1}^{\tau_2} \Psi(z) \left| \frac{E(\tau)}{E_{\max}} \right|^2 \exp[-4\alpha z] d\tau. \quad (52)$$

The limits of the integration depend upon the duration of the envelope function $E(t)$ for $\tau_1 < \tau < \tau_2$.

The numerical model shown here has material properties of aluminum with cubic crystals of $450 \mu\text{m}$ as the mean grain diameter. The elastic constants are $C_{11} = 103.4 \text{ GPa}$, $C_{12} = 57.1 \text{ GPa}$, $C_{44} = 28.6 \text{ GPa}$, and the density is $\rho = 2,700 \text{ kg/m}^3$. The model is tested for various frequencies ranging from 5 to 12 MHz. The input signal is broadband consisting of three cycles. Since the proposed theory shown in Eq. (24) was derived for a single frequency input wave, the output signal is filtered at the desired frequency $f \pm 1 \text{ MHz}$. Experiments can be performed for a wide band signal and the scattered response can be extracted for the required frequency limits. This will minimize the number of simulations performed when data are required at variable frequencies. Since the pressure load of uniform magnitude is applied, an effective focus is created in the material. The focal depth is calculated from a Voronoi model with homogeneous crystal properties and used an input to the theoretical model.

The numerical results are obtained from 100 realizations of the Voronoi polycrystal model. Each realization is constructed randomly and represents a single transducer location with respect to the real experimental

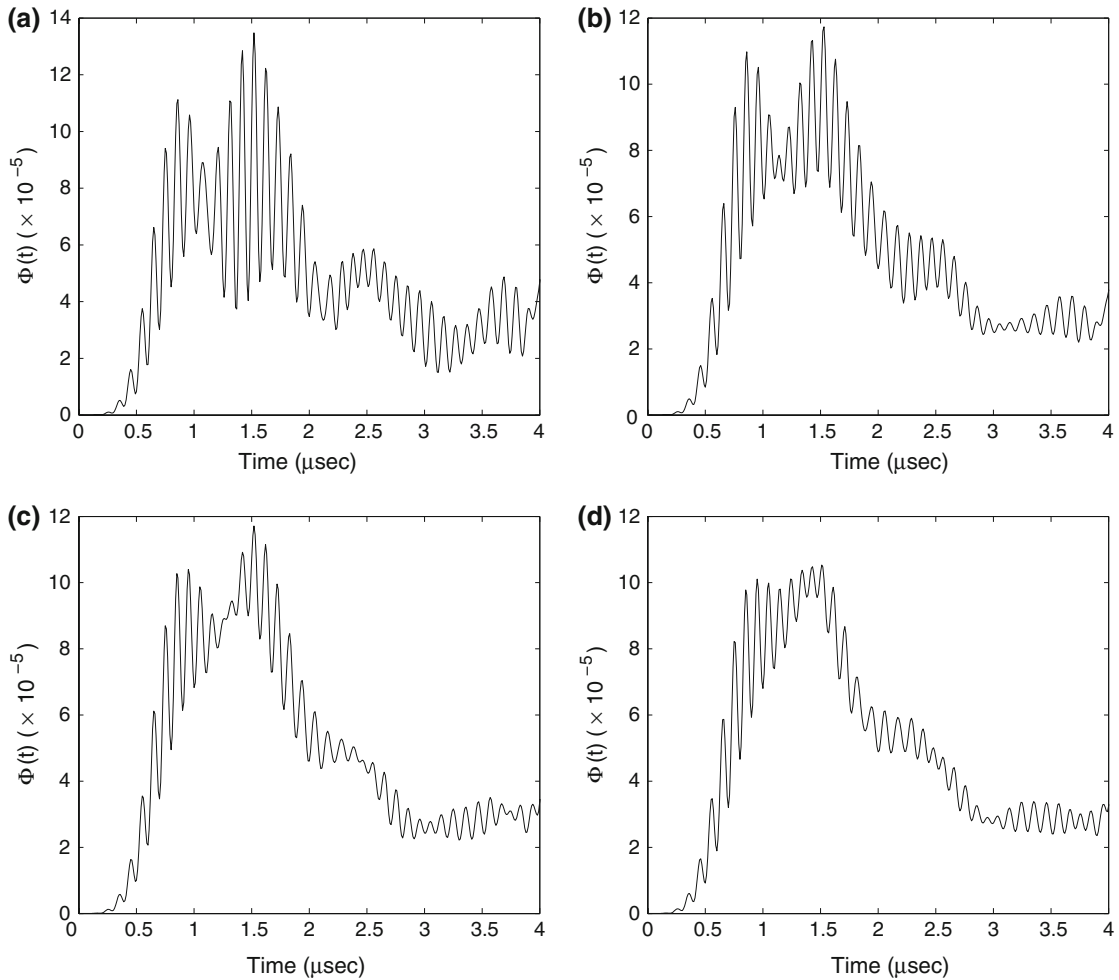


Fig. 5 Spatial variance from **a** 25, **b** 50, **c** 75, and **d** 100 realizations for aluminum using 5 MHz input wave frequency

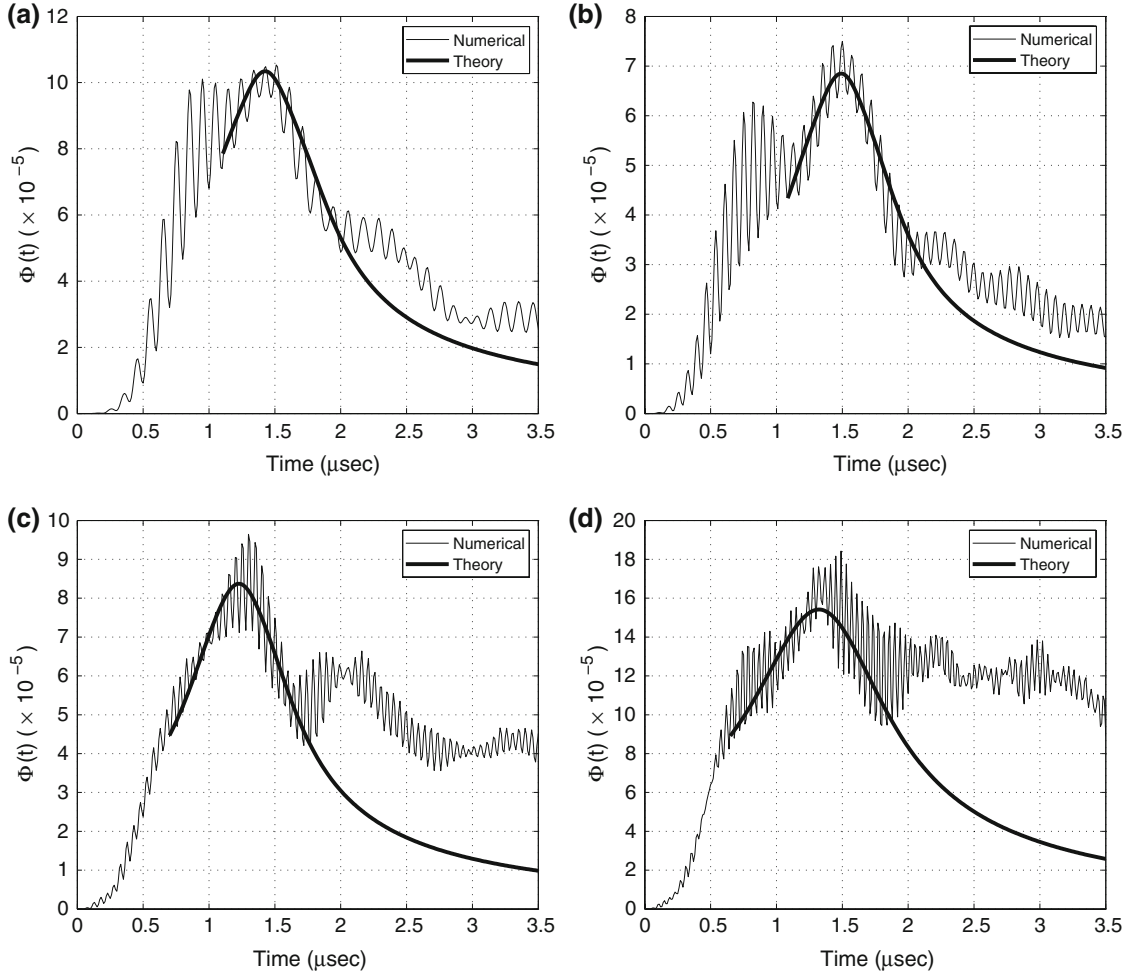


Fig. 6 Numerical and theoretical scattered response for aluminum at **a** 5 MHz, **b** 7 MHz, **c** 10 MHz, **d** 12 MHz of input wave frequency

setup. The fluctuations in the numerical results decrease with increasing number of realizations. The scattered response for different numbers of realizations is shown in Fig. 5. The results from 75 to 100 realizations are approximately similar. Hence all the subsequent results shown are based on 100 realizations. It should be noted that the number of realizations of the Voronoi model required to achieve acceptable accuracy may depend on the material properties or the input wave frequencies.

The scattered response using the filtered signal is shown in Fig. 6. The theoretical model is denoted by the thicker line of the two. The results are obtained for input frequencies of 5, 7, 10 and 12 MHz shown in Fig. 6a–d, respectively. For low frequencies, it is expected that the scattering is governed by the mean grain volume [22]. Thus, we may write

$$\bar{V} = \int d^3r e^{-r/L} = 8\pi L^3, \quad (53)$$

where $\bar{V} = \frac{1}{6}\pi D^3$. Equation (53) implies a low-frequency relation given as $L = 0.28D$. At higher frequency, Weaver [22] speculated that $\eta(\omega)$ depends on the volume density of the grain boundaries rather than the grain volume. In this case, the correlation length may be half of the value calculated from Eq. (53). However, it is evident that the appropriate length scale may also depend upon the degree of scattering, an aspect that highlights the lack of precision in the form of the relationship between L and D . In order to study the connection between L and D , the numerical results were fit to the theory (for the best value of L) by minimizing the root mean square deviation of the error between the theoretical and numerical scattered response. Here, to match the numerical with the theoretical results we find that $L/D = 1.6, 1.6, 1.1$ and 0.5 times the mean grain

diameter for input frequencies 5, 7, 10 and 12 MHz, respectively. This result clearly suggests that single crystal anisotropy affects the correlation length. This constant decreases as the degree of scattering in the material increases. The technical reasons for these variations in L are out of scope of this work, but the numerical model can be very useful for investigating this relation. The influence of the form of the correlation function on the interpretation of the scattered response is evident from these results.

The numerical results show good agreement with the two dimensional backscatter model derived here. The dependence of the correlation on the frequency of the input shows an interesting phenomenon that should be investigated in detail for different materials and a broader range of frequencies using the numerical model shown here.

4 Summary

In this article, a theoretical model for the scattered response for polycrystalline materials in a two-dimensional domain was derived. This model was compared with a numerical polycrystalline model constructed using Voronoi tessellation. The numerical and theoretical results are compared with each other for aluminum. The results are presented for an input wave at various frequencies. The numerical results have been adjusted by varying the correlation length. At low frequency the correlation length is 1.6 times the mean grain diameter. As the frequency increases the correlation length shows a decreasing trend. The numerical results show that the correlation length is 1.6, 1.6, 1.1 and 0.5 times the mean grain diameter at 5, 7, 10 and 12 MHz, respectively. These results are consistent with previously attenuation calculations [26] using the same Voronoi model. The numerical model shown here can be easily used to investigate the frequency dependence of the correlation length for complex materials or multi-phase materials, where a theoretical model does not exist.

Acknowledgments The support of the Department of Energy and Federal Railroad Administration for this research is gratefully acknowledged. The authors also thank Dr. R. Bruce Thompson and Dr. Frank J. Margetan from Iowa State University for conversations regarding this work.

References

- Holmes, A.K., Challis, R.E., Wedlock, D.J.: A wide bandwidth study of ultrasound velocity and attenuation in suspensions: comparison of theory with experimental measurements. *J. Colloid Interface Sci.* **156**, 261–268 (1993)
- Greenwood, M.S., Mai, J.L., Good, M.S.: Attenuation measurements of ultrasound in a kaolin-water slurry: a linear dependence on frequency. *J. Acoust. Soc. Am.* **94**, 908–916 (1993)
- Hovem, J.M., Ingram, G.D.: Viscous attenuation of sound in saturated sand. *J. Acoust. Soc. Am.* **66**, 1807–1812 (1979)
- Sayers, C.M., Grenfell, R.L.: Ultrasonic propagation through hydrating cements. *Ultrasonics* **31**, 147–153 (1993)
- Biot, M.: Theory of propagation of elastic waves in a fluid saturated porous solid I and II. *J. Acoust. Soc. Am.* **28**, 168–191 (1956)
- Wu, D., Qian, Z.W., Shao, D.: Sound attenuation in a coarse granular medium. *J. Sound Vib.* **162**, 529–535 (1993)
- Courtney, R.C., Mayer, L.: Acoustic properties of fine grained sediments. *J. Acoust. Soc. Am.* **93**, 3193–3200 (1993)
- Goddard, J.D.: Nonlinear elasticity and pressure dependent wave speeds in granular media. *Proc. R. Soc. Lond. A* **430**, 105–131 (1990)
- Cook, B.D., Arnoult III, W.J.: Gaussian–Laguerre/Hermite formulation for the nearfield of an ultrasonic transducer. *J. Acoust. Soc. Am.* **59**, 9–11 (1976)
- Gubernatis, J.E., Domany, E., Krumhansl, J.A.: Formal aspects of the theory of the scattering of ultrasound by flaws in elastic materials. *J. Appl. Phys.* **48**, 2804–2811 (1977)
- Thompson, R.B., Gray, T.A.: A model relating ultrasonic scattering measurement through liquid–solid interfaces to unbounded medium scattering amplitudes. *J. Acoust. Soc. Am.* **74**(4), 1279–1290 (1983)
- Margetan, F.J., Gray, T.A., Thompson, R.B.: A technique for quantitative measuring microstructurally induced ultrasonic noise. In: Thompson, D.O., Chimenti, D.E. (eds.) *Review of Progress in Quantitative NDE.*, vol. 10. Plenum Press, New York, pp. 1721–1728 (1991)
- Thompson, R.B., Margetan, F., Haldipur, P., Yu, L., Li, A., Panetta, P., Wasan, H.: Scattering of elastic waves in simple and complex polycrystals. *Wave Motion* **45**, 655–674 (2008)
- Ghoshal, G., Turner, J.A., Weaver, R.L.: Wigner distribution of a transducer beam pattern within a multiple scattering formalism for heterogeneous solids. *J. Acoust. Soc. Am.* **122**, 2009–2021 (2007)
- ABAQUS: Superior Finite Element Analysis Solutions. ABAQUS, Pawtucket (2003)
- Ghoshal, G.: Numerical simulations of elastic wave scattering in polycrystalline materials. Master's thesis, University of Nebraska-Lincoln (2003)
- Yang, L., Ghoshal, G., Turner, J.A.: Ultrasonic scattering in textured polycrystalline materials, *Advanced ultrasonic methods for material and structure inspection.* Hermes Science Publishing, UK (2007)
- Rogers, P.H., Buren, A.L.V.: An exact expression for the Lommel diffraction correction integral. *J. Acoust. Soc. Am.* **55**, 724–728 (1974)

19. Ruiz, M.A., Nagy, P.B.: Diffraction correction for precision surface acoustic wave velocity measurements. *J. Acoust. Soc. Am.* **112**, 835–842 (2002)
20. Frisch, U.: Wave propagation in random media. In: Barucha-Reid, A.T. (ed.) *Probabilistic Methods in Applied Mathematics*, vol. 1, pp. 75–198. Academic, New York (1968)
21. Achenbach, J.D.: *Wave Propagation in Elastic Solids*. Elsevier, New York (1984)
22. Weaver, R.L.: Diffusivity of ultrasound in polycrystals. *J. Mech. Phys. Solids* **38**(1), 55–86 (1990)
23. Schmerr, L.W.: A multigaussian ultrasonic beam model for high performance simulation on a personal computer. *Mater. Eval.* **58**, 882–888 (2000)
24. Thompson, R.B., Gray, T.A., Rose, J.H., Kogan, V.G., Lopes, E.F.: The radiation of elliptical and bicylindrically focused piston transducers. *J. Acoust. Soc. Am.* **82**, 1818–1828 (1987)
25. Thompson, R.B., Lopes, E.F.: The effects of focusing and refraction on Gaussian ultrasonic beams. *J. Nondestruct. Eval.* **4**, 107–123 (1984)
26. Ghoshal, G., Turner, J.A.: Numerical model of longitudinal wave scattering in polycrystals. *IEEE Trans. Ultrason. Ferroelectr. Freq. Control* (2009, to appear)